BULLETIN OF THE POLISH ACADEMY OF SCIENCES
TECHNICAL SCIENCES, Vol. 74(6), 2026, Article number: 3057
DOI: 10.24425/bpasts.2026.3057

Unified study of model-informed extensions of ADRC and state-feedback control with integral compensator

Mikołaj MROTEK* **and Stefan BROCK**

Faculty of Control, Robotics and Electrical Engineering, Institute of Robotics and Machine Intelligence, Poznan University of Technology, Piotrowo 3a, 60-965 Poznan, Poland

Abstract. This paper investigates generalized model-informed extensions of active disturbance rejection control (ADRC) and disturbance-centric state-feedback control with integral compensator (IDRC). Four control structures are considered, including literature-established matrix-based generalized ADRC, previously proposed regression-based generalized ADRC, and their IDRC counterparts employing corresponding embedding mechanisms. Closed-loop transfer-function representations and parametric Routh–Hurwitz stability analyses are derived for second- and third-order integrating systems with a single inertia term under model uncertainty and observer bandwidth variations. The obtained results indicate that the embedding mechanism has a significant influence on closed-loop robustness. In particular, regression-based formulations improve stability properties for relatively slow observers but may become more sensitive to modeling errors and phase lag for large observer bandwidths. The consistency of these trends is additionally confirmed for a third-order Ball Balancing Table system including measurement filtering. Experimental results obtained on a real laboratory setup remain consistent with the predicted stability regions and confirm similar robustness relationships for both ADRC- and IDRC-based structures.

Keywords: active disturbance rejection control; state-feedback control; stability analysis; model-informed control; disturbance-centric control.

1. INTRODUCTION

Active disturbance rejection control (ADRC) has become a widely recognized control methodology for uncertain dynamical systems due to its disturbance-centric formulation and relatively low dependence on accurate plant models. In its classical linear form, the plant is usually approximated by an integral-chain model, while unknown dynamics, modeling errors, and external disturbances are lumped into a total disturbance estimated by an extended state observer (ESO) [1, 2]. The bandwidth-parameterization framework further increased the practical accessibility of ADRC by providing simple tuning rules based on the desired controller and observer dynamics [3].

Although ADRC was originally promoted as a model-free or weakly model-dependent methodology, recent developments have shown that additional plant information can be systematically incorporated into the ADRC design. Such model-informed ADRC structures aim to improve transient performance, robustness, and applicability to more demanding systems, while preserving the disturbance rejection mechanism of the original approach. In this context, the known information usually concerns the order of the plant, the input gain, or selected coefficients of the nominal characteristic polynomial. The idea of using known plant information in linear ADRC was investigated, among others, in [4, 5], where the controller and observer gains were modified according to available model parameters.

Related developments have also considered generalized disturbance estimation structures, disturbance-observer-based interpretations, and implementation-oriented ADRC formulations accounting for practical robustness limitations, including filtering, sampling, and actuator constraints [6–9]. These studies indicate that the manner in which nominal model information is incorporated into the control loop may affect closed-loop robustness and implementation properties.

More broadly, disturbance estimation and compensation have also been extensively investigated within the disturbance-observer-based control (DOBC) framework, where nominal plant models are incorporated into observer-based compensation loops. Although DOBC and ADRC originate from different design philosophies, both rely on estimating and compensating the lumped effect of model uncertainties and external disturbances, highlighting the importance of how nominal model information is embedded into the control structure [10–12].

At the same time, several studies have emphasized that ADRC should not be treated as a single fixed control structure, but rather as a disturbance-rejection-oriented design philosophy that admits different realizations and interpretations. Transfer-function and implementation-oriented analyses have helped clarify the relationship between ADRC and classical frequency-domain control concepts [13, 14]. Other works have shown equivalences or close structural relationships between ADRC and standard industrial controllers, including PID-like formulations and

*e-mail: mikolaj.mrotek@put.poznan.pl

Manuscript submitted 2026-06-04, revised 2026-07-01, initially accepted for publication 2026-07-26, published in November 2026.

© 2026 The Author(s). This is an open access article under the CC BY license (http://creativecommons.org/licenses/by/4.0/)

disturbance-observer-based control schemes [15, 16]. This line of research is important because it reduces the conceptual gap between ADRC and established control theory.

A related perspective was developed by the authors in [17], where classical state-feedback control with an integral compensator was revisited from the ADRC viewpoint in the non-model-informed case. The resulting integral disturbance rejection control (IDRC) interpretation showed that, although IDRC does not explicitly estimate the total disturbance, the integral action can play a similar disturbance-rejection role for constant or slowly varying disturbances. This provided a backward-compatibility link between ADRC and classical state-space control with integral action.

In parallel, the regression-based generalized ADRC structure previously introduced by the authors in [18] demonstrated that the way in which nominal model information is embedded into the controller has a significant impact on closed-loop stability. Specifically, two embedding mechanisms can be distinguished. In the matrix-based formulation, the nominal plant dynamics are directly included in the observer and controller matrices. In the regression-based formulation, the same model information is introduced through additional regression terms, while the nominal integral-chain structure and the corresponding gain-selection rules are preserved. Although both approaches use the same nominal model, they may lead to different internal controller dynamics, zero locations, and stability conditions.

These observations motivate the main question addressed in this work: if classical ADRC and IDRC can exhibit similar disturbance-rejection behavior, can the same model-informed embedding mechanisms be consistently extended from ADRC to IDRC? Answering this question is important for two reasons. First, it verifies whether the disturbance-centric interpretation of IDRC remains valid beyond the basic integral-chain case. Second, it allows one to assess whether the robustness effects previously observed for generalized ADRC structures also appear in state-feedback control with integral action.

While integral state-feedback control itself is classical, its generalized disturbance-centric formulation employing regression-based model embedding, according to the best of the authors' knowledge, has not been previously reported. Therefore, this paper presents a unified comparative study of four model-informed disturbance rejection control structures: LGADRCa, LGADRCb, GIDRCa, and GIDRCb, described later in detail. Unlike previous studies focused separately on LGADRC and IDRC-ADRC equivalence (in the non-model-informed version), the present work demonstrates that the influence of the embedding mechanism constitutes a structural property that extends across different disturbance-rejection-oriented control architectures. The considered methods differ in two independent aspects: the underlying control philosophy, namely ADRC versus state-feedback control with integral action, and the mechanism used to incorporate nominal model information, namely matrix-based versus regression-based embedding. This distinction is important because it allows separating the influence of the embedding mechanism from the particular disturbance-compensation paradigm, thereby enabling a more general robustness-oriented interpretation of model-informed disturbance rejection control.

The main contributions of this paper are as follows:

1. A unified formulation of model-informed ADRC and IDRC structures using both matrix-based and regression-based embedding mechanisms.
2. Derivation of equivalent closed-loop transfer-function representations for all considered methods, enabling direct structural comparison between ADRC- and IDRC-based formulations.
3. Extension of the embedding-mechanism analysis previously reported for generalized ADRC structures to generalized IDRC formulations, including parametric Routh–Hurwitz stability analysis for both second- and third-order integrating plants with a single inertia term under model uncertainty and observer bandwidth variations.
4. Demonstration that the influence of the embedding mechanism constitutes a structural property preserved across both ADRC- and IDRC-based control architectures exhibiting similar disturbance-rejection properties.
5. Extension of the stability analysis to the third-order Ball Balancing Table system including measurement filtering, confirming that the robustness trends associated with the embedding mechanism remain consistent also in practical implementation conditions.
6. Experimental validation on a real Ball Balancing Table system, demonstrating consistency between the predicted stability regions and the observed closed-loop behavior of all considered control structures.

2. DESCRIPTION OF METHODS

We consider the following model of the SISO LTI plant:

$$y^{(n)} = -\underline{\hat{\theta}}^{\mathrm{T}}\,\underline{\phi} + \hat{b}\,u + f^{*}(\cdot), \tag{1}$$

where $\underline{\phi} = \left[y, \dot{y}, \ldots, y^{(n-1)}\right]^{\mathrm{T}}$ is the regression vector, $\underline{\hat{\theta}} = [\hat{a}_0, \hat{a}_1, \ldots, \hat{a}_{n-1}]^{\mathrm{T}}$ are the estimated coefficients of the linear drift, and $\hat{b}$ is the estimated input gain. The total disturbance of the system is denoted by $f^{*}(\cdot)$ and has the following representation

$$f^{*}(\cdot) = \left(\underline{\hat{\theta}}^{\mathrm{T}} - \underline{\theta}^{\mathrm{T}}\right)\underline{\phi} + \left(b - \hat{b}\right)u + bw, \tag{2}$$

with the real system parameters $\underline{\theta} = [a_0, a_1, \ldots, a_{n-1}]^{\mathrm{T}}$, the exact input gain b and the external disturbance w.

Introducing the state vector $\underline{x} = \underline{\phi}$ for model (1), the following state-space representation can be obtained

$$\begin{cases} \dot{\underline{x}} = \mathbf{A}\underline{x} - \underline{b}\underline{\hat{\theta}}^{\mathrm{T}}\underline{x} + \underline{b}\left(\hat{b}u + f^{*}(\cdot)\right), \\ y = \underline{c}^{\mathrm{T}}\underline{x}, \end{cases} \tag{3}$$

where $\mathbf{A} = \begin{bmatrix} \underline{0}_{n-1\times 1} & \mathbf{I}_{n-1\times n-1} \\ & \underline{0}_{1\times n} \end{bmatrix} \in \mathscr{R}^{n\times n}$, $\underline{b} = \begin{bmatrix} \underline{0}_{n-1\times 1} \\ 1 \end{bmatrix} \in \mathscr{R}^{n}$, $\underline{c}^{\mathrm{T}} = \begin{bmatrix} 1 & \underline{0}_{1\times n-1} \end{bmatrix} \in \mathscr{R}^{n}$.

The state-space representation (3) can be used in ADRC/IDRC synthesis in the following ways:

- Matrix-based embedding:

$$\dot{\underline{x}} = \left(\mathbf{A} - \underline{b}\,\hat{\underline{\theta}}^{\mathrm{T}}\right)\underline{x} + \underline{b}\left(\hat{b}\,u + f^*(\cdot)\right), \tag{4}$$

  therefore, the term $\mathbf{A} - \underline{b}\,\hat{\underline{\theta}}^{T}$ represents the state matrix of the system.
- Regression-based embedding:

$$\dot{\underline{x}} = \mathbf{A}\underline{x} + \underline{b}\left(\hat{b}\,u - \hat{\underline{\theta}}^{T}\underline{x} + f^*(\cdot)\right), \tag{5}$$

  where the system matrix remains the integrator chain and the drift is introduced using the regression form. The key difference between both formulations lies in the way the nominal plant dynamics are incorporated into the control structure. In the matrix-based formulation, the nominal dynamics modify the system matrix directly, whereas in the regression-based formulation they are introduced as an additional algebraic term.

2.1. ADRC structures

- LGADRCa: For the extended representation of (4), namely $\underline{z} = \left[\underline{x}^T, f^*\right]^T$, we design the ESO in the following form

$$\dot{\hat{\underline{z}}} = \left(\mathbf{A}_e - \underline{b}_e\hat{\underline{\theta}}_e^{\mathrm{T}} - \underline{l}^{(a)}\,\underline{c}_e^{\mathrm{T}}\right)\hat{\underline{z}} + \hat{b}\,\underline{b}_e\,u + \underline{l}^{(a)}y, \tag{6}$$

  with $\underline{l}^{(a)} \in \mathscr{R}^{n+1}$ being the observer gains vector. For tracking a smooth trajectory $\underline{r} = \left[y_r \quad \dot{y}_r \quad \cdots \quad y_r^{(n-1)}\right]^{\mathrm{T}}, y_r^{(n)}$, the following control law can be derived

$$u = \hat{b}^{-1}\left(\underline{k}^{(a)\mathrm{T}}\left(\underline{r} - \hat{\underline{x}}\right) + y_r^{(n)} + \hat{\underline{\theta}}^{\mathrm{T}}\,\underline{r} - \hat{f}^*(\cdot)\right). \tag{7}$$

- LGADRCb: In this case, the observer takes the form

$$\dot{\hat{\underline{z}}} = \left(\mathbf{A}_e - \underline{l}^{(b)}\,\underline{c}_e^{T}\right)\hat{\underline{z}} + \underline{b}_e\left(\hat{b}\,u - \hat{\underline{\theta}}_e^{T}\hat{\underline{z}}\right) + \underline{l}^{(b)}y, \tag{8}$$

  where $\underline{l}^{(b)}$ is the gain vector. The control law for trajectory tracking yields

$$u = \hat{b}^{-1}\left(\underline{k}^{(b)\mathrm{T}}\left(\underline{r} - \hat{\underline{x}}\right) + y_r^{(n)} + \hat{\underline{\theta}}^{\mathrm{T}}\,\hat{\underline{x}} - \hat{f}^*(\cdot)\right). \tag{9}$$

In equations (6), (8) the matrices are as follows:

$$\mathbf{A}_e = \begin{bmatrix}\mathbf{A} & \underline{b}\\ \underline{0}_{1\times n+1}\end{bmatrix} \in \mathscr{R}^{n+1\times n+1},\quad \underline{b}_e = \begin{bmatrix}\underline{b}\\ 0\end{bmatrix} \in \mathscr{R}^{n+1\times 1},$$

$$\underline{c}_e^{\mathrm{T}} = \begin{bmatrix}\underline{c}^{\mathrm{T}} & 0\end{bmatrix} \in \mathscr{R}^{1\times n+1},\quad \hat{\underline{\theta}}_e^{\mathrm{T}} = \begin{bmatrix}\hat{\underline{\theta}}^{\mathrm{T}} & 0\end{bmatrix} \in \mathscr{R}^{1\times n+1}.$$

It should be noted that the estimated extended state is defined as $\hat{\underline{z}} = \left[\hat{\underline{x}}^{\mathrm{T}} \quad \hat{f}^*\right]^{\mathrm{T}}$. Consequently, the control laws in (7) and (9) are expressed directly in terms of the estimated plant states $\hat{\underline{x}}$ and the estimated total disturbance $\hat{f}^*$, i.e., the corresponding components of the estimated extended state $\hat{\underline{z}}$. The detailed derivations of both model-informed ADRC structures can be found in [18].

2.2. IDRC structures

In the IDRC approach the total disturbance of the system (1) is not used in the design of the controller explicitly, but integral action is employed to compensate disturbances for which $f^*(\cdot)$ is approximately constant. Since the LGADRCa and LGADRCb structures are explicitly defined by equations (6)–(9) and discussed in detail in [18], Fig. 1 illustrates the corresponding generalized IDRC structures, thereby emphasizing the extension of the model-embedding mechanisms from ADRC to state-feedback control with integral action. Based on [17], the state-space representation (4) can be used in IDRC synthesis in the following ways:

- GIDRCa: The state of the system (4) is estimated via a Luenberger state observer (SO)

$$\dot{\hat{\underline{x}}} = \left(\mathbf{A} - \underline{b}\hat{\underline{\theta}}^{\mathrm{T}} - \underline{\iota}^{(a)}\underline{c}^{\mathrm{T}}\right)\hat{\underline{x}} + \underline{b}\hat{b}u + \underline{\iota}^{(a)}y, \tag{10}$$

  where $\underline{\iota}^{(a)} \in \mathscr{R}^n$ contains the observer gains. The control law for trajectory tracking yields

$$u = \hat{b}^{-1}\left(\underline{\kappa}^{(a)\mathrm{T}}\left(\underline{r} - \hat{\underline{x}}\right) + \hat{\underline{\theta}}^{\mathrm{T}}\underline{r} + y_r^{(n)} + \kappa_{\mathrm{int}}^{(a)}\int_0^t \left(y_r(\tau) - y(\tau)\right)\mathrm{d}\tau\right), \tag{11}$$

  where $\underline{\kappa}_e^{(a)} = \left[\underline{\kappa}^{(a)\mathrm{T}}, \kappa_{\mathrm{int}}^{(a)}\right]^{\mathrm{T}} \in \mathscr{R}^{n+1}$ is the controller gains vector with $\kappa_{\mathrm{int}}^{(a)}$ denoting the integral path gain. Introducing the extended state variable $q = \int_0^t \left(y_r(\tau) - y(\tau)\right)\mathrm{d}\tau$ and assuming $\hat{\underline{x}} \approx \underline{x}$, the nominal closed-loop dynamics can be written as

$$\begin{bmatrix}\dot{\underline{x}}\\ \dot{q}\end{bmatrix} = \underbrace{\begin{bmatrix}\mathbf{A} - \underline{b}\left(\underline{\kappa}^{(a)\mathrm{T}} + \hat{\underline{\theta}}^{\mathrm{T}}\right) & \underline{b}\kappa_{\mathrm{int}}^{(a)}\\ -\underline{c}^{\mathrm{T}} & 0\end{bmatrix}}_{\mathbf{H}_{\mathrm{CL}}^{\mathrm{GIDRCa}}}\begin{bmatrix}\underline{x}\\ q\end{bmatrix} + \begin{bmatrix}\underline{b}\left(\underline{\kappa}^{(a)\mathrm{T}} + \hat{\underline{\theta}}^{\mathrm{T}}\right) & \underline{b}\\ \underline{c}^{\mathrm{T}} & 0\end{bmatrix}\begin{bmatrix}\underline{r}\\ y_r^{(n)}\end{bmatrix}, \tag{12}$$

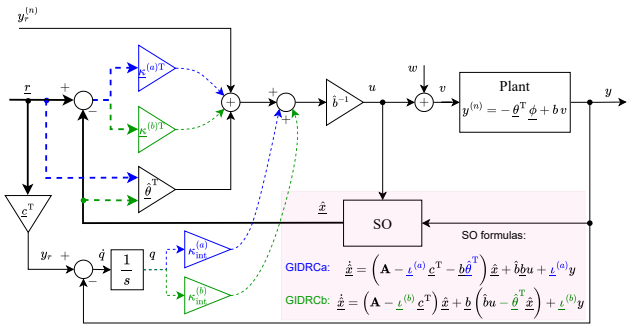

Fig. 1. Comparison of control structures for the considered generalized IDRC variants. Blue elements correspond to the matrix-based GIDRCa formulation, whereas green elements denote the regression-based GIDRCb structure

where

$$\mathbf{H}_{\mathrm{CL}}^{\mathrm{GIDRCa}} = \begin{bmatrix} \mathbf{A} - \underline{b}\left(\underline{\kappa}^{(a)\mathrm{T}} + \underline{\hat{\theta}}^{\mathrm{T}}\right) & \underline{b}\kappa_{\mathrm{int}}^{(a)} \\ -\underline{c}^{\mathrm{T}} & 0 \end{bmatrix} \tag{13}$$

yields the closed-loop state matrix.

- GIDRCb: The SO for model (5) yields

$$\dot{\underline{\hat{x}}} = \left(\mathbf{A} - \underline{\iota}^{(b)}\underline{c}^{\mathrm{T}}\right)\underline{\hat{x}} + \underline{b}\left(\hat{b}u - \underline{\hat{\theta}}^{T}\underline{\hat{x}}\right) + \underline{\iota}^{(b)}y, \tag{14}$$

where $\underline{\iota}^{(b)} \in \mathscr{R}^n$ denotes the vector of observer gains, and the control law is given by

$$u = \hat{b}^{-1}\Bigg(\underline{\kappa}^{(b)\mathrm{T}}\left(\underline{r} - \underline{\hat{x}}\right) + \underline{\hat{\theta}}^{\mathrm{T}}\underline{\hat{x}} + y_r^{(n)} + \kappa_{\mathrm{int}}^{(b)}\int_0^t \left(y_r(\tau) - y(\tau)\right)\mathrm{d}\tau\Bigg), \tag{15}$$

Introducing the extended state variable $q = \int_0^t (y_r(\tau) - y(\tau))\,\mathrm{d}\tau$ and assuming $\underline{\hat{x}} \approx \underline{x}$, the nominal closed-loop dynamics can be written as

$$\begin{bmatrix} \dot{\underline{x}} \\ \dot{q} \end{bmatrix} = \underbrace{\begin{bmatrix} \mathbf{A} - \underline{b}\underline{\kappa}^{(b)^{\mathrm{T}}} & \underline{b}\kappa_{\mathrm{int}}^{(b)} \\ -\underline{c}^{\mathrm{T}} & 0 \end{bmatrix}}_{\mathbf{H}_{\mathrm{CL}}^{\mathrm{GIDRCb}}} \begin{bmatrix} \underline{x} \\ q \end{bmatrix} + \begin{bmatrix} \underline{b}\underline{\kappa}^{(b)^{\mathrm{T}}} & \underline{b} \\ \underline{c}^{\mathrm{T}} & 0 \end{bmatrix} \begin{bmatrix} \underline{r} \\ y_r^{(n)} \end{bmatrix}, \tag{16}$$

where

$$\mathbf{H}_{\mathrm{CL}}^{\mathrm{GIDRCb}} = \begin{bmatrix} \mathbf{A} - \underline{b}\underline{\kappa}^{(b)\mathrm{T}} & \underline{b}\kappa_{\mathrm{int}}^{(b)} \\ -\underline{c}^{\mathrm{T}} & 0 \end{bmatrix} \tag{17}$$

yields the state matrix of the closed-loop system.

2.3. Gains selection

In the ADRC-based variants, the controller and observer gains are chosen to satisfy the following pole-placement conditions:

- LGADRCa:

$$\begin{aligned} \det\left(s\mathbf{I}_n - \left(\mathbf{A} - \underline{b}\underline{\hat{\theta}}^{T} - \underline{b}\,\underline{k}^{(a)\mathrm{T}}\right)\right) &= (s+\omega_c)^n, \\ \det\left(s\mathbf{I}_{n+1} - \left(\mathbf{A}_e - \underline{b}_e\underline{\hat{\theta}}_e^{T} - \underline{l}^{(a)}\,\underline{c}_e^{T}\right)\right) &= (s+\omega_o)^{n+1}, \end{aligned} \tag{18}$$

- LGADRCb

$$\begin{aligned} \det\left(s\mathbf{I}_n - \left(\mathbf{A} - \underline{b}\,\underline{k}^{(b)\mathrm{T}}\right)\right) &= (s+\omega_c)^n, \\ \det\left(s\mathbf{I}_{n+1} - \left(\mathbf{A}_e - \underline{l}^{(b)}\,\underline{c}_e^{T}\right)\right) &= (s+\omega_o)^{n+1}. \end{aligned} \tag{19}$$

The detailed formulas for the observer and controller gains of both LGADRC variants, including the relations between the (a) and (b) structures, are reported in [18] and are not repeated here.

In the IDRC-based variants, the gain selection follows the same pole-placement principle, applied now to the state observer and to the closed-loop matrix defined by the integral action.

- GIDRCa:

$$\begin{aligned} \det\left(s\mathbf{I}_n - \left(\mathbf{A} - \underline{b}\underline{\hat{\theta}}^{\mathrm{T}} - \underline{\iota}^{(a)}\underline{c}^{\mathrm{T}}\right)\right) &= (s+\omega_o)^n, \\ \det\left(s\mathbf{I}_{n+1} - \mathbf{H}_{\mathrm{CL}}^{\mathrm{GIDRCa}}\right) &= (s+\omega_c)^n(s+\beta\omega_c). \end{aligned} \tag{20}$$

- GIDRCb

$$\begin{aligned} \det\left(s\mathbf{I}_n - \left(\mathbf{A} - \underline{\iota}^{(b)}\underline{c}^{\mathrm{T}}\right)\right) &= (s+\omega_o)^n, \\ \det\left(s\mathbf{I}_{n+1} - \mathbf{H}_{\mathrm{CL}}^{\mathrm{GIDRCb}}\right) &= (s+\omega_c)^n(s+\beta\omega_c). \end{aligned} \tag{21}$$

In these formulas, ω_c and ω_o denote the desired closed-loop and observer bandwidths, respectively, and β is the factor resulting from the shift of one of the poles as non-dominant (parameterization proposed in [17]).

For the regression-based variant GIDRCb, the solution of (21) yields

$$\kappa_j^{(b)} = \left[\beta\binom{n}{j} + \binom{n}{j-1}\right]\omega_c^{n-j+1}, \qquad j = 1,\ldots,n, \tag{22}$$

and the integral gain

$$\kappa_{\mathrm{int}}^{(b)} = \beta\,\omega_c^{n+1}. \tag{23}$$

For the matrix-based variant GIDRCa, it can be derived that the gains are related to those of GIDRCb through

$$\underline{\kappa}^{(a)} = \underline{\kappa}^{(b)} - \underline{\hat{\theta}}, \tag{24}$$

which directly corresponds to the LGADRCa/b relationship reported in [18]. Importantly, the integral gain remains identical for both variants

$$\kappa_{\mathrm{int}}^{(a)} = \kappa_{\mathrm{int}}^{(b)} = \kappa_{\mathrm{int}} = \beta\,\omega_c^{n+1}. \tag{25}$$

For the regression-based GIDRCb observer, the state matrix retains the integral-chain structure, thus $\underline{\iota}^{(b)}$ can be obtained via

$$\iota_i^{(b)} = \binom{n}{i}\omega_o^i, \qquad i = 1,\ldots,n, \tag{26}$$

which is directly analogous to the ESO tuning formula for the LGADRCb variant. For the matrix-based GIDRCa observer, the characteristic polynomial can be expressed as

$$\underline{\alpha} = \mathbf{T}\left(\underline{\hat{\theta}}\right)\underline{\iota}^{(a)} + \underline{\gamma}\left(\underline{\hat{\theta}}\right), \tag{27}$$

where $\underline{\alpha} \in \mathbb{R}^n$ collects the coefficients of the polynomial and

$$\mathbf{T}\left(\underline{\hat{\theta}}\right) = \begin{bmatrix} 1 & 0 & \cdots & 0 \\ \hat{a}_{n-1} & 1 & \cdots & 0 \\ \hat{a}_{n-2} & \hat{a}_{n-1} & \ddots & 0 \\ \vdots & \vdots & \ddots & 1 \\ \hat{a}_1 & \hat{a}_2 & \cdots & 1 \end{bmatrix}, \quad \underline{\gamma}\left(\underline{\hat{\theta}}\right) = \begin{bmatrix} \hat{a}_{n-1} \\ \hat{a}_{n-2} \\ \vdots \\ \hat{a}_0 \end{bmatrix}$$

are the lower–triangular Toeplitz-like matrix and $\underline{\hat{\theta}}$, written in the reverse order. It is worth noting that $T(\hat{\theta})$ and $\gamma(\hat{\theta})$ retain the same definitions in both ADRC and IDRC formulations. Enforcing the desired polynomial leads to the affine relation

$$\underline{\iota}^{(a)} = \mathbf{T}\left(\underline{\hat{\theta}}\right)^{-1}\left(\underline{\iota}^{(b)} - \underline{\gamma}\left(\underline{\hat{\theta}}\right)\right),$$

which is the counterpart of the LGADRCa/b observer-gain transformation reported in [18]. The presented gain relationships reveal that both ADRC and IDRC variants preserve analogous structural dependencies between the matrix-based and regression-based formulations.

3. THEORETICAL ANALYSIS OF ADRC AND IDRC

3.1. Transfer function analysis

The structural differences between the matrix-based and regression-based embedding mechanisms become apparent when transfer functions are derived from the corresponding observer and control laws. In what follows, we present the closed-loop representations for all four considered variants: LGADRCa, LGADRCb, GIDRCa, and GIDRCb. A constant reference value y_r is assumed, so $y_r^{(i)} = 0$ for $i = 1, \ldots, n$. Denoting its Laplace transform by $Y_r(s)$, each of the four control schemes can be written as

$$U(s) = \hat{b}^{-1}\left(G_{\mathrm{PF}}(s)Y_r(s) - G_{\mathrm{FB}}(s)Y(s)\right). \tag{28}$$

We can also define

$$\begin{aligned}
\mathbf{A}^{(a)}_{cl,\ \mathrm{ADRC}} &= \mathbf{A}_e - \underline{b}_e\underline{\hat{\theta}}_e^{\mathrm{T}} - \underline{l}^{(a)}\underline{c}_e^{\mathrm{T}} - \underline{b}_e\underline{k}_e^{(a)\mathrm{T}},\\
\mathbf{A}^{(b)}_{cl,\ \mathrm{ADRC}} &= \mathbf{A}_e - \underline{l}^{(b)}\underline{c}_e^{\mathrm{T}} - \underline{b}_e\underline{k}_e^{(b)\mathrm{T}},\\
\mathbf{A}^{(a)}_{cl,\ \mathrm{IDRC}} &= \mathbf{A} - \underline{b}\underline{\hat{\theta}}^{\mathrm{T}} - \underline{\iota}^{(a)}\underline{c}^{\mathrm{T}} - \underline{b}\underline{\kappa}^{(a)\mathrm{T}},\\
\mathbf{A}^{(b)}_{cl,\ \mathrm{IDRC}} &= \mathbf{A} - \underline{\iota}^{(b)}\underline{c}^{\mathrm{T}} - \underline{b}\underline{\kappa}^{(b)\mathrm{T}}.
\end{aligned} \tag{29}$$

For the LGADRC variants, we introduce the extended controller gain vector $\underline{k}_e^{(*)} = \left[\underline{k}^{(*)\mathrm{T}}, 1\right]^{\mathrm{T}}$, which enables merging the state – feedback action with disturbance rejection. Here, $(*)$ denotes the selected LGADRC variant, i.e., (a) or (b). The derived transfer functions $G_{\mathrm{PF}}(s)$ and $G_{\mathrm{FB}}(s)$ for all considered model-informed methods are collected in Table 1. The formulas for the basic versions of both approaches (IDRC and LADRC), under the assumption of a chain-of-integrators model, were reported in [17].

3.2. Problem formulation

Consider the following second-order integrating plant and its nominal approximation

$$G_p(s) = \frac{b}{s^2 + a_1 s}, \quad \hat{G}_p(s) = \frac{b}{s^2 + \hat{a}_1 s}, \tag{30}$$

where the input gain is assumed to be known exactly, i.e., $\hat{b} = b$. All control schemes considered in this paper – LGADRCa, LGADRCb, GIDRCa, and GIDRCb – admit an equivalent two-degree-of-freedom (2-DOF) input–output representation, separating reference shaping and feedback stabilization. Accordingly, the plant, feedback, and prefilter transfer functions are written as

$$G_p(s) = \frac{b}{D_p(s)}, \ G_{\mathrm{FB}}(s) = \frac{N_{\mathrm{FB}}(s)}{D_{\mathrm{FB}}(s)}, \ G_{\mathrm{PF}}(s) = \frac{N_{\mathrm{PF}}(s)}{D_{\mathrm{PF}}(s)}. \tag{31}$$

Additionally, the desired bandwidth ratio $c = \omega_o/\omega_c$ was introduced in the considerations. For each of the four model-informed ADRC/IDRC variants, the transfer functions $G_{\mathrm{PF}}(s)$ and $G_{\mathrm{FB}}(s)$ are derived using the estimated model (30). As summarized in Table 1, the prefilter and feedback paths share a common internal denominator,

$$D_{\mathrm{PF}}(s) = D_{\mathrm{FB}}(s) = D_{\mathrm{C}}(s), \tag{32}$$

which characterizes the internal controller dynamics of the given scheme.

Consequently, although each method gives rise to two distinct controller transfer functions (G_{PF} and G_{FB}), only four different controller denominator polynomials appear – one for each considered structure. The corresponding numerators $N_{\mathrm{PF}}(s)$ and $N_{\mathrm{FB}}(s)$ depend on the selected embedding mechanism and are reported explicitly in Table 1. The obtained transfer functions reveal that the influence of the embedding mechanism on the controller structure is preserved consistently across both ADRC and IDRC formulations. Moreover, analogous modifications of the internal controller dynamics can be observed for the matrix-based and regression-based variants, which motivates the subsequent comparative stability analysis.

3.3. Closed-loop transfer function

We consider the standard 2-DOF closed-loop interconnection induced by the control law (28) and a matched external disturbance w entering additively at the plant input. The plant output then satisfies

$$Y(s) = G_p(s)(U(s) + W(s)). \tag{33}$$

Substituting (28) into (33) and collecting terms yields

$$\begin{aligned}
Y(s)\left(1 + \hat{b}^{-1}G_p(s)G_{\mathrm{FB}}(s)\right) &= \hat{b}^{-1}G_p(s)G_{\mathrm{PF}}(s)Y_r(s)\\
&\quad + G_p(s)W(s).
\end{aligned} \tag{34}$$

The closed-loop mapping from the reference signal to the output is given by

$$\begin{aligned}
G_{yr}(s) = \frac{Y(s)}{Y_r(s)} &= \frac{\hat{b}^{-1}G_p(s)G_{\mathrm{PF}}(s)}{1 + \hat{b}^{-1}G_p(s)G_{\mathrm{FB}}(s)}\\
&= \frac{N_{\mathrm{PF}}(s)D_{\mathrm{FB}}(s)}{D_{\mathrm{PF}}(s)\,\varphi(s)} \overset{(32)}{=} \frac{N_{\mathrm{PF}}(s)}{\varphi(s)},
\end{aligned} \tag{35}$$

where

$$\varphi(s) = D_p(s)D_{\mathrm{FB}}(s) + N_{\mathrm{FB}}(s) \tag{36}$$

yields the closed-loop system polynomial.

Table 1
Transfer functions $G_{\mathrm{PF}}(s)$ and $G_{\mathrm{FB}}(s)$ for all considered methods

Method	$G_{\mathrm{PF}}(s)$	$G_{\mathrm{FB}}(s)$
LGADRCa	$\frac{\left(k_1^{(a)}+\hat{a}_0\right)\left(\det\left(s\mathbf{I}-\mathbf{A}_{cl,\ \mathrm{ADRC}}^{(a)}\right)-\underline{k}_e^{(a)\mathrm{T}}\mathrm{adj}\left(s\mathbf{I}-\mathbf{A}_{cl,\ \mathrm{ADRC}}^{(a)}\right)\underline{b}_e\right)}{\det\left(s\mathbf{I}-\mathbf{A}_{cl,\ \mathrm{ADRC}}^{(a)}\right)}$	$\frac{\underline{k}_e^{(a)\mathrm{T}}\mathrm{adj}\left(s\mathbf{I}-\mathbf{A}_{cl,\ \mathrm{ADRC}}^{(a)}\right)\underline{l}^{(a)}}{\det\left(s\mathbf{I}-\mathbf{A}_{cl,\ \mathrm{ADRC}}^{(a)}\right)}$
LGADRCb	$\frac{k_1^{(b)}\left(\det\left(s\mathbf{I}-\mathbf{A}_{cl,\ \mathrm{ADRC}}^{(b)}\right)+(\underline{\hat{\theta}}_e^{\mathrm{T}}-\underline{k}_e^{(b)\mathrm{T}})\mathrm{adj}\left(s\mathbf{I}-\mathbf{A}_{cl,\ \mathrm{ADRC}}^{(b)}\right)\underline{b}_e\right)}{\det\left(s\mathbf{I}-\mathbf{A}_{cl,\ \mathrm{ADRC}}^{(b)}\right)}$	$\frac{\left(\underline{k}_e^{(b)\mathrm{T}}-\underline{\hat{\theta}}_e^{\mathrm{T}}\right)\mathrm{adj}\left(s\mathbf{I}-\mathbf{A}_{cl,\ \mathrm{ADRC}}^{(b)}\right)\underline{l}^{(b)}}{\det\left(s\mathbf{I}-\mathbf{A}_{cl,\ \mathrm{ADRC}}^{(b)}\right)}$
GIDRCa	$\frac{\left(s\kappa_1^{(a)}+s\hat{a}_0+\kappa_{\mathrm{int}}\right)\left(\det\left(s\mathbf{I}-\mathbf{A}_{cl,\ \mathrm{IDRC}}^{(a)}\right)-\underline{\kappa}^{(a)\mathrm{T}}\mathrm{adj}\left(s\mathbf{I}-\mathbf{A}_{cl,\ \mathrm{IDRC}}^{(a)}\right)\underline{b}\right)}{s\det\left(s\mathbf{I}-\mathbf{A}_{cl,\ \mathrm{IDRC}}^{(a)}\right)}$	$\frac{\underline{\kappa}^{(a)\mathrm{T}}\mathrm{adj}\left(s\mathbf{I}-\mathbf{A}_{cl,\ \mathrm{IDRC}}^{(a)}\right)\left(s\underline{\iota}^{(a)}-\underline{b}\kappa_{\mathrm{int}}\right)+\kappa_{\mathrm{int}}\det\left(s\mathbf{I}-\mathbf{A}_{cl,\ \mathrm{IDRC}}^{(a)}\right)}{s\det\left(s\mathbf{I}-\mathbf{A}_{cl,\ \mathrm{IDRC}}^{(a)}\right)}$
GIDRCb	$\frac{\left(s\kappa_1^{(b)}+\kappa_{\mathrm{int}}\right)\left(\det\left(s\mathbf{I}-\mathbf{A}_{cl,\ \mathrm{IDRC}}^{(b)}\right)+\left(\underline{\hat{\theta}}^{\mathrm{T}}-\underline{\kappa}^{(b)\mathrm{T}}\right)\mathrm{adj}\left(s\mathbf{I}-\mathbf{A}_{cl,\ \mathrm{IDRC}}^{(b)}\right)\underline{b}\right)}{s\det\left(s\mathbf{I}-\mathbf{A}_{cl,\ \mathrm{IDRC}}^{(b)}\right)}$	$\frac{\left(\underline{\kappa}^{(b)\mathrm{T}}-\underline{\hat{\theta}}^{\mathrm{T}}\right)\mathrm{adj}\left(s\mathbf{I}-\mathbf{A}_{cl,\ \mathrm{IDRC}}^{(b)}\right)\left(s\underline{\iota}^{(b)}-\underline{b}\kappa_{\mathrm{int}}\right)+\kappa_{\mathrm{int}}\det\left(s\mathbf{I}-\mathbf{A}_{cl,\ \mathrm{IDRC}}^{(b)}\right)}{s\det\left(s\mathbf{I}-\mathbf{A}_{cl,\ \mathrm{IDRC}}^{(b)}\right)}$

3.4. Routh–Hurwitz analysis

To assess the stability properties of the closed-loop systems, a Routh–Hurwitz analysis was performed. The characteristic polynomial of each structure can be written in the unified form

$$\varphi(s) = s^5 + \alpha_4 s^4 + \alpha_3 s^3 + \alpha_2 s^2 + \alpha_1 s + \alpha_0, \tag{37}$$

where the coefficients α_i follow directly from (36). For a fifth-order polynomial, the first column of the Routh array is given by

$$\begin{aligned} r_1 &= 1, \\ r_2 &= \alpha_4, \\ r_3 &= \frac{r_2\alpha_3 - \alpha_2}{r_2}, \\ r_4 &= \frac{r_3\alpha_2 - \alpha_4 b_2}{r_3}, \\ r_5 &= \frac{r_4 b_2 - r_3\alpha_0}{r_4}, \\ r_6 &= \alpha_0, \end{aligned} \tag{38}$$

where $b_2 = \dfrac{r_2\alpha_1 - \alpha_0}{r_2}$. The necessary and sufficient condition for stability is that all elements of the first column satisfy $r_i > 0$. To enable a parametric study, the model uncertainty in the inertia coefficient and the normalized observer bandwidth are parameterized as

$$\hat{a}_1 = a_1(1+d), \qquad p = \frac{\omega_o}{\hat{a}_1}. \tag{39}$$

With this parameterization, the coefficients α_i become functions of the parameters d and p. For each Routh condition $r_i > 0$, a corresponding critical value $p_{\mathrm{crit}}^{(i)}(d,c)$ is defined as the smallest value of p for which the condition is satisfied, i.e.,

$$r_i\left(p_{\mathrm{crit}}^{(i)}, d, c\right) = 0. \tag{40}$$

The overall stability boundary is then determined by the most restrictive condition

$$p_{\mathrm{crit}}^{\star}(d,c) = \max_i \left(p_{\mathrm{crit}}^{(i)}(d,c)\right), \tag{41}$$

which guarantees that all Routh conditions are simultaneously satisfied. The analysis was repeated for a range of practically relevant bandwidth ratios $c \in [3,20]$. For each triplet (p,d,c), the critical value $p_{\mathrm{crit}}^{\star}(d,c)$ was computed numerically by evaluating all Routh conditions and selecting the most restrictive one. The resulting stability conditions, shown in Fig. 2, provide a three-dimensional representation of the admissible observer bandwidth. This visualization reveals how the stability margin evolves jointly with model uncertainty and observer tuning.

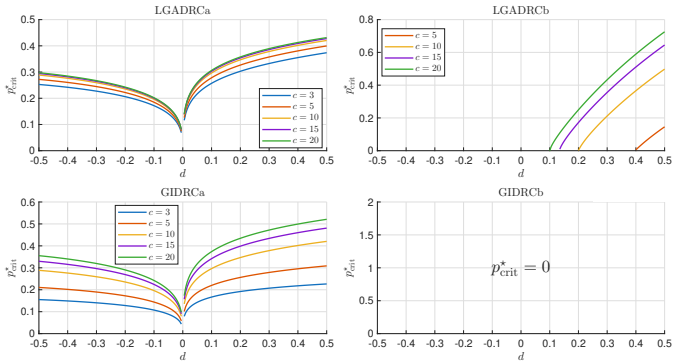

Fig. 2. Stability boundaries obtained for the second-order nominal model ($n = 2$) using the Routh–Hurwitz analysis. The curves indicate the minimum observer-bandwidth ratio required to satisfy all Routh–Hurwitz stability conditions under the considered model uncertainty

To generalize the findings obtained for the second-order model and extend the conclusions of [18], an analogous stability analysis was performed for the third-order system. The considered integrating plant and its nominal approximation are given by

$$G_p(s) = \frac{b}{s^3 + a_2 s^2}, \qquad \hat{G}_p(s) = \frac{b}{s^3 + \hat{a}_2 s^2},$$

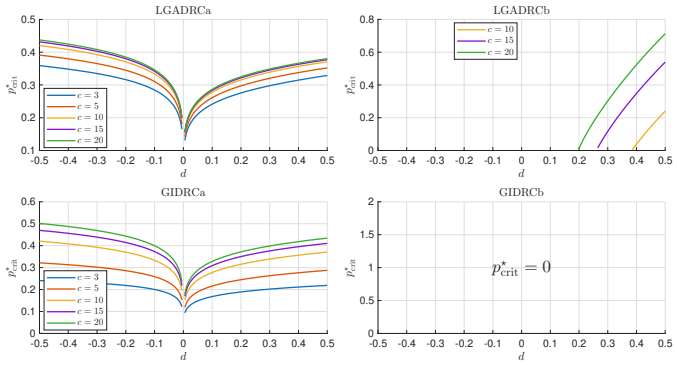

Fig. 3. Stability boundaries obtained for the third-order model ($n = 3$), corresponding to the BBT system dynamics. The curves indicate the minimum observer-bandwidth ratio required to satisfy all Routh–Hurwitz stability conditions under the considered model uncertainty

while the model uncertainty in the inertia coefficient and the normalized observer bandwidth are parameterized according to

$$\hat{a}_2 = a_2(1+d), \qquad p = \frac{\omega_o}{\hat{a}_2}.$$

This parameterization enables a direct comparison of the stability trends between the second- and third-order cases.

Key observations. The analysis for both second- and third-order models reveals consistent trends:

- The apparent termination of several stability-boundary curves at $d = 0$ corresponds to the nominal case, for which the assumed model matches the plant exactly. Consequently, the closed-loop system achieves the desired dynamics, and no positive lower bound on the observer-bandwidth ratio p is imposed.
- Matrix-based variants (LGADRCa, GIDRCa) exhibit a finite stability boundary $p^*_c rit(d,c)$, which depends on both d and c.
- Regression-based GIDRCb remains stable over the entire investigated parameter range.
- The stability properties of LGADRCb strongly depend on the operating region and may deteriorate for specific combinations of (d,c).
- Increasing the observer bandwidth (c) does not always improve stability and may lead to degradation, particularly for the LGADRCb structure.

These results indicate that the mechanism used to incorporate model knowledge (matrix-based vs. regression-based) has a direct impact on the parametric robustness of the closed-loop system. It should be emphasized that the presented stability analysis, performed for both second- and third-order plants, is conducted under idealized assumptions, i.e., without measurement filtering, sensor noise, actuator saturation, or digital implementation effects. Consequently, the obtained results should be interpreted primarily as a structural robustness study intended to reveal general trends associated with the considered embedding mechanisms, rather than as a complete implementation-level stability assessment.

4. BALL BALANCING TABLE (BBT)

Experiments were conducted on a real 2-DoF Ball Balancing Table (BBT) system, shown in Fig. 4. The experimental platform is based on the ACROME Ball Balancing Table system [19] equipped with two RC servo motors actuating the table inclination along the x- and y-axes and a resistive touchscreen used for ball position measurement. The control algorithms were implemented in MATLAB/Simulink and executed in real time using the Arduino Mega 2560 platform.

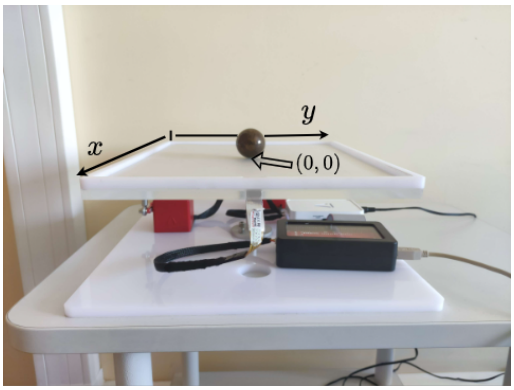

Fig. 4. Experimental setup of the Ball Balancing Table (BBT) system used for validation

For control design, the nonlinear system dynamics can be approximated by the following nominal model:

$$\hat{G}_p(s) = \frac{\hat{b}}{s^3 + \hat{a}_2 s^2}, \tag{42}$$

where $\hat{b} = 750$ and $\hat{a}_2 = 25$. The BBT system is particularly suitable for validating the considered control structures, as its dynamics correspond to a chain-of-integrators with a single nonzero coefficient, which enables direct verification of the theoretical stability predictions derived in Section 3.

5. EXPERIMENTS

The experiments were designed to evaluate the influence of the observer bandwidth on closed-loop stability and performance, with particular emphasis on the differences between matrix-based and regression-based model embedding.

Two experimental scenarios were considered, both based on nominal model parameters ($n = 3$, $\hat{b} = 750$, $\hat{a}_0 = \hat{a}_1 = 0$, $\hat{a}_2 = 25$, $\omega_c = 2.8$). For both GIDRC variants, the additional parameter was set to $\beta = 10$.

For all compared methods:

1) fast observer: $\omega_o = 15\omega_c = 42$ $(c = 15)$, $\omega_o = 1.68\hat{a}_{n-1}$ $(p = 1.68)$
2) slow observer: $\omega_o = 3\omega_c = 8.4$ $(c = 3)$, $\omega_o = 0.336\hat{a}_{n-1}$ $(p = 0.336)$

The controller bandwidth was selected as the highest practically achievable value that did not excite severe mechanical constraints or persistent actuator saturation on the experimental

setup. The observer bandwidth ratio (c) was selected according to standard ADRC tuning practice [3] in order to investigate both moderate and aggressive disturbance estimation scenarios.

The control input corresponds to the angular displacement of the servo mechanism and is subject to saturation constraints:

$$-36 \le u \le 36 \text{ deg}. \tag{43}$$

In the real-world implementation, due to measurement noise and quantization effects originating from the touchscreen sensor, first-order low-pass filtering was introduced in the feedback path

$$G_f(s) = \frac{20}{s+20}.$$

The filter was necessary to suppress high-frequency chattering from the sensor. The additional phase lag introduced by this filter affects the stability of the closed-loop system for large observer bandwidths and was therefore included in the extended stability analysis presented in Fig. 5.

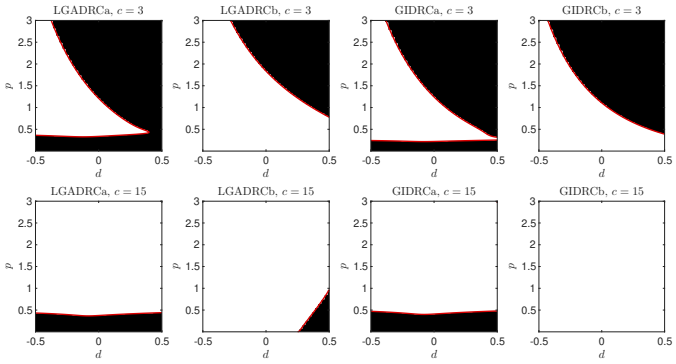

Fig. 5. Stability analysis for third-order model with measurement filtering. White regions indicate stable operating points obtained from the parametric analysis, while black regions correspond to instability

The experimental time responses for both observer settings are presented in Figs. 6 and 7, whereas the quantitative comparison is summarized in Table 2 using the performance indices

$$J_{\text{ITAE}} = \int_0^T t\,|y(t) - y_r(t)|\,\mathrm{d}t,$$

$$J_u = \int_0^T u^2(t)\,\mathrm{d}t.$$

The experimental results remain consistent with the theoretical stability analysis performed for the third-order model with measurement filtering. Notably, the obtained responses confirm that the robustness properties are strongly influenced by the selected embedding mechanism.

For the slow-observer case, the regression-based LGADRCb structure preserves stable operation in operating regions where the matrix-based LGADRCa variant becomes oscillatory, which is consistent with the stability maps shown in Fig. 5.

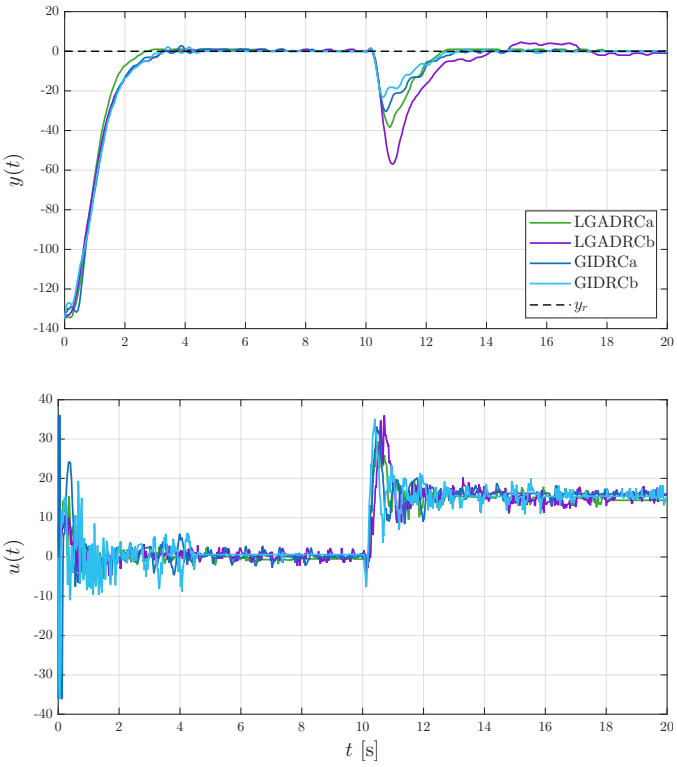

Fig. 6. Closed-loop responses for the fast observer case ($\omega_o = 15\omega_c$)

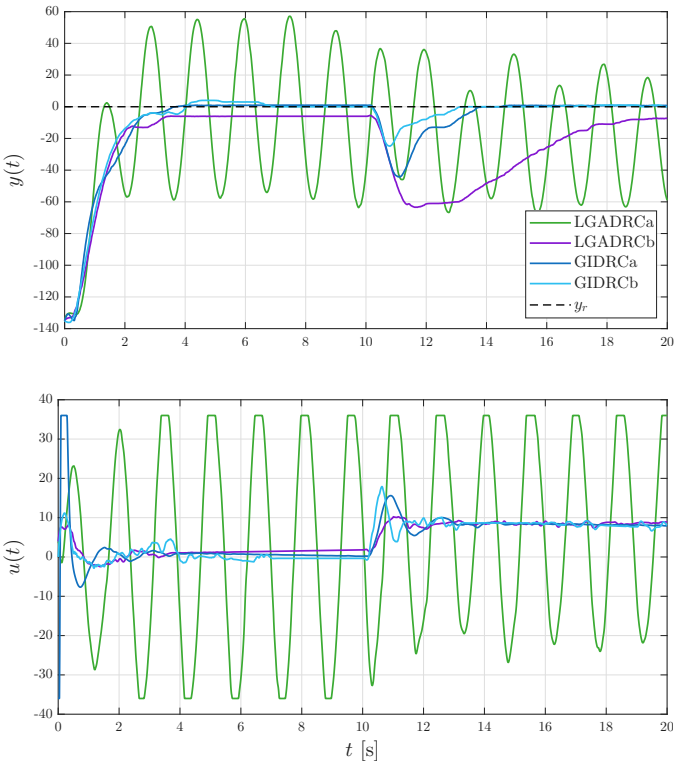

Fig. 7. Closed-loop responses for the slow observer case ($\omega_o = 3\omega_c$)

This observation extends the conclusions previously reported for second-order systems to the considered third-order BBT setup.

Table 2
Performance indices obtained in the BBT experiments

Method	Fast observer		Slow observer	
	J_{ITAE}	$10^3 J_u$	J_{ITAE}	$10^3 J_u$
LGADRCa	605.90	**2.481**	6326.30	11.971
LGADRCb	1125.50	2.616	4803.10	**0.739**
GIDRCa	531.11	3.008	972.19	1.150
GIDRCb	**436.75**	2.708	**542.26**	0.788

At the same time, the results obtained for larger observer bandwidths confirm that increasing the observer speed does not necessarily improve robustness. In particular, in the presence of measurement filtering, the regression-based LGADRCb formulation becomes more sensitive to positive model mismatch ($d > 0$) in the high-bandwidth region, while the remaining methods preserve larger stability margins in this part of the parameter space. This effect is also consistent with the parametric stability analysis including measurement filtering.

Additionally, the quantitative performance indices reported in Table 2 remain consistent with the qualitative observations from Figs. 6 and 7. In particular, the GIDRCb structure achieves the lowest J_{ITAE} values for both observer settings, confirming its favorable transient performance. At the same time, the obtained J_u values indicate that the improvement in tracking quality is not always accompanied by the lowest control effort, illustrating the expected trade-off between control performance and actuator activity.

The obtained results additionally indicate that the choice of the embedding mechanism becomes practically important whenever the observer bandwidth cannot be increased arbitrarily due to implementation constraints such as hardware limitations, measurement noise, filtering, or sampling limitations. Under such realistic conditions, the robustness differences between the matrix-based and regression-based formulations become significant and should therefore be considered already at the controller synthesis stage. In particular, the generalized IDRC formulations can offer practical advantages in such applications by preserving accurate steady-state regulation and effective rejection of slowly varying disturbances even for relatively low observer bandwidths.

6. CONCLUSIONS

This paper presented a unified study of model-informed extensions of ADRC and state-feedback control with integral action within a disturbance-rejection-oriented framework.

The obtained results demonstrated that the mechanism used to incorporate nominal model information plays a fundamental role in shaping closed-loop robustness properties. In particular, both ADRC- and IDRC-based formulations preserve similar structural relationships between matrix-based and regression-based embedding mechanisms. These relationships were consistently observed at the state-space, transfer-function, and stability-analysis levels for both second- and third-order systems.

The performed stability analysis and experimental validation revealed a characteristic robustness trade-off associated with the regression-based embedding mechanism. Specifically, the LGADRCb structure exhibited improved stability properties for relatively slow observers, confirming and extending the conclusions previously reported for second-order systems. For larger observer bandwidths, the regression-based formulation became more sensitive to modeling errors, particularly to positive mismatch ($d > 0$) in the presence of measurement filtering and implementation-related phase lag. Importantly, the extended stability analysis including the measurement filter remained consistent with the experimentally observed stability regions of the real BBT system.

Table 3
Practical synthesis guidelines derived from the theoretical and experimental results

Design step	Guideline
	Choice of structure
LGADRCa	Preferred when a relatively fast observer (large $p = \omega_o/\hat{a}_{n-1}$) can be employed. For lower values of p, the stability region becomes more restrictive.
LGADRCb	Provides improved stability properties for relatively slow observers (small p), but may become sensitive to modeling errors and filtering-induced phase lag for relatively large observer bandwidths (large p).
GIDRCa	Shows trends similar to LGADRCa, with slightly improved stability regions for relatively slow observers.
GIDRCb	Provides the widest stability regions in the analyzed cases and the best overall experimental performance, particularly for relatively slow observers and significant model uncertainty.
	Tuning
Controller bandwidth ω_c	Select according to the open-loop plant dynamics and physical limitations of the setup. In practice, ω_c is often limited by mechanical constraints, resonances, actuator saturation, or other implementation-related factors. For the generalized IDRC structures, the additional integral state increases the closed-loop order by one; therefore, one additional pole is typically placed at $-\beta\omega_c$, where $\beta \in [5, 15]$.
Observer bandwidth ω_o	Tune according to the standard bandwidth-ratio rule, typically $\omega_o = c\omega_c$ with $c \in [3, 20]$. The terms "slow" and "fast" observer should be interpreted relative to the normalized ratio $p = \omega_o/\hat{a}_{n-1}$ rather than the absolute observer bandwidth. A relatively fast observer is recommended whenever implementation constraints (e.g., measurement noise, filtering, sampling rate) do not restrict the achievable observer bandwidth. Otherwise, a relatively slow observer should be adopted, with the choice of the embedding mechanism becoming increasingly important for preserving robustness.

The findings additionally confirm that generalized IDRC formulations exhibit robustness trends similar to their ADRC counterparts despite relying on a different disturbance-compensation mechanism based on integral action rather than explicit disturbance estimation. Moreover, the experiments indicated that the generalized IDRC variants may offer practical advantages in applications where the observer bandwidth cannot be increased arbitrarily due to sampling, hardware, or noise limitations, since the integral-action-based disturbance compensation preserves accurate steady-state regulation even for relatively slow observers.

Overall, the findings suggest that the embedding mechanism should be treated as a robustness-oriented design choice rather than merely an implementation detail. The presented framework may therefore provide useful guidelines for selecting model-informed disturbance-rejection structures depending on the expected operating conditions, admissible observer bandwidth, and uncertainty level.

The above results can be translated into practical synthesis guidelines summarized in Table 3. The table should be interpreted as a qualitative design aid rather than a universal tuning rule, since the final choice of ω_c, ω_o, and the control structure depends on the plant dynamics, implementation constraints, and the expected level of model uncertainty.

ACKNOWLEDGEMENTS

This work was supported by 0214/SBAD/0251.

REFERENCES

[1] Z. Gao, Y. Huang, and J. Han, "An alternative paradigm for control system design," in *Proceedings of the 40th IEEE conference on decision and control (Cat. No. 01CH37228)*, vol. 5. IEEE, 2001, pp. 4578–4585.

[2] Z. Gao, "Active disturbance rejection control: a paradigm shift in feedback control system design," in *2006 American Control Conference*. IEEE, 2006, pp. 2399–2405.

[3] Z. Gao, "Scaling and bandwidth-parameterization based controller tuning," in *ACC*, 2003, pp. 4989–4996, doi: 10.1109/ACC.2003.1242516.

[4] R. Zhou and W. Tan, "A generalized active disturbance rejection control approach for linear systems," in *2015 IEEE 10th Conference on Industrial Electronics and Applications (ICIEA)*. IEEE, 2015, pp. 248–255, doi: 10.1109/ICIEA.2015.7334120.

[5] C. Fu and W. Tan, "Tuning of linear ADRC with known plant information," *ISA Trans.*, vol. 65, p. 384–393, 2016, doi: 10.1016/j.isatra.2016.06.016.

[6] A. Sobhy and D. Lei, "Model-assisted active disturbance rejection controller for maximum efficiency schemes of dfig-based wind turbines," *Int. Trans. Electr. Energy Syst.*, vol. 31, no. 11, p. e13107, 2021.

[7] D. Wu, K. Yuan, Y. Huang, Z.-M. Yuan, and L. Hua, "Design and test of an improved active disturbance rejection control system for water sampling unmanned surface vehicle," *Ocean Eng.*, vol. 245, p. 110367, 2022.

[8] J. Jugo, A. Elejaga, and P. Echevarria, "Modified active disturbance rejection control scheme for systems with time delay," *IET Control Theory Appl.*, vol. 17, no. 14, pp. 1992–2003, 2023.

[9] S. Jain and Y.V. Hote, "Predictive generalized active disturbance rejection control for fractional order systems with time delay," *J. Dyn. Syst. Meas. Control*, vol. 145, no. 7, p. 071003, 2023.

[10] W.-H. Chen, J. Yang, L. Guo, and S. Li, "Disturbance-observer-based control and related methods – an overview," *IEEE Trans. Ind. Electron.*, vol. 63, no. 2, pp. 1083–1095, 2016.

[11] G. Park and J. Back, "Survey of disturbance observer-based controller and related challenging problems," *J. Inst. Control Robot. Syst.*, vol. 30, no. 4, pp. 363–372, 2024.

[12] A.H. Kahsay, P. Derugo, K. Szabat, and S. Katsura, "Design of disturbance observer-based robust speed control structure for two-mass drive system with the help of birch optimization algorithm," *Energies*, vol. 18, no. 8, p. 1914, 2025.

[13] G. Herbst, "Transfer function analysis and implementation of active disturbance rejection control," *Control Theory Technol.*, vol. 19, pp. 19–34, 2021.

[14] G. Herbst and R. Madonski, "Tuning and implementation variants of discrete-time ADRC," *Control Theory Technol.*, vol. 21, pp. 72–88, 2023, doi: 10.1007/s11768-023-00127-0.

[15] R. Madonski, S. Shao, H. Zhang, Z. Gao, J. Yang, and S. Li, "General error-based active disturbance rejection control for swift industrial implementations," *Control Eng. Pract.*, vol. 84, pp. 218–229, 2019.

[16] R. Madonski, G. Herbst, and M. Stankovic, "ADRC in output and error form: Connection, equivalence, performance," *Control Theory Technol.*, vol. 21, pp. 56–71, 2023, doi: 10.1007/s11768-023-00129-y.

[17] M. Mrotek, J. Michalski, R. Madonski, D. Pazderski, and M. Retinger, "Towards backward compatibility of ADRC: revisiting classical state-feedback control with integral compensator," *Bull. Pol. Acad. Sci. Tech. Sci.*, vol. 73, no. 2, p. e152608, 2025, doi: 10.24425/bpasts.2024.152608.

[18] M. Mrotek, J. Michalski, R. Madonski, D. Pazderski, M. Retinger, and P. Kozierski, "Balancing benefits and risks of embedding system knowledge in linear active disturbance rejection control," *Electronics*, vol. 14, no. 22, p. 4467, 2025, doi: 10.3390/electronics14224467.

[19] *Ball balancing table – user manual, Version 2021.1*, Acrome, 2021.